THE JOURNAL OF PHYSICAL CHEMISTRY B

Article

Cite This: J. Phys. Chem. B 2020, 124, 173−180

pubs.acs.org/JPCB

Origin of Unusually High Fluorescence Anisotropy of 3-Hydroxyflavone in Water: Formation of Probe−Solvent Cage-like Cluster

Sinjan Das,[†] Suman Chakrabarty,[‡] and Nitin Chattopadhyay*[,†]

[†]Department of Chemistry, Jadavpur University, Kolkata 700 032, India

[‡]Department of Chemical, Biological & Macromolecular Sciences, S. N. Bose National Centre for Basic Sciences, Kolkata 700 106, India

Supporting Information

ABSTRACT: Based on the unusually high fluorescence anisotropy (FA) of 3-hydroxyflavone (3HF) in water medium in contrast to the very low FA of its methoxy counterpart (3MF), our proposition invoked formation of an intermolecular hydrogen-bonded cage-like probe−solvent cluster of 3HF in water. In the present work, ab-initio DFT-based quantum chemical calculations have been exploited to provide a foundation for our interpretation. Ground-state optimization of 3HF with varying numbers of water molecules leads to the formation of a cage-like or loop-like probe−water cluster. Our calculations reveal that the structures with four to five water molecules are stabilized to the maximum extent. Classical molecular dynamics simulations reveal that the rotational dynamics of 3HF is much slower in water compared to that in alkane medium, which also goes in favor of the probe−solvent cluster formation in water medium. Apart from the theoretical studies, an indirect experimental approach has been adopted to substantiate formation of the probe−water cluster. The atypical observation of reduced FA of 3HF entrapped in micelles relative to that of the fluorophore in water implies disruption of the probe−water cluster with the addition of micelles, corroborating our original proposition of formation of an intermolecularly hydrogen-bonded 3HF−water cluster.

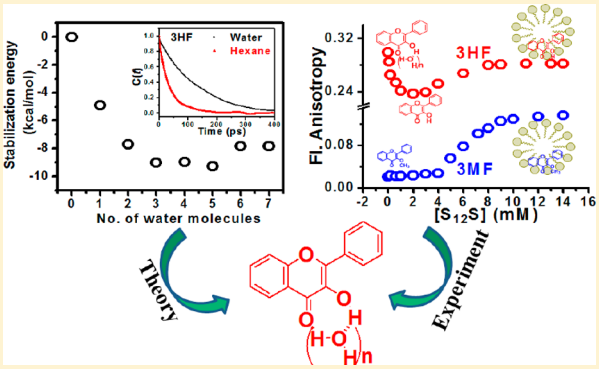

1. INTRODUCTION

During the last four decades, extensive research based on both experimental and theoretical approaches has established that the photophysical behavior of 3-hydroxyflavone (3HF) (Scheme 1), the backbone of the flavonoid class of compounds and a spectroscopically important molecular system, is largely governed by its ability to undergo intramolecular proton transfer in the photoexcited state in homogeneous as well as microheterogeneous environments.[1−12] Due to the biological importance of the flavonoid systems as antioxidants[13] and their abundance in the vegetable kingdom, understanding the solution-phase behavior of 3HF is still a thriving topic of interest to the global research community. Despite being a well-studied molecular system, the fluorescence polarization behavior of 3HF has not been explored systemically.

Scheme 1. Schematic Structures of 3HF, 3MF, and Solvated 3HF

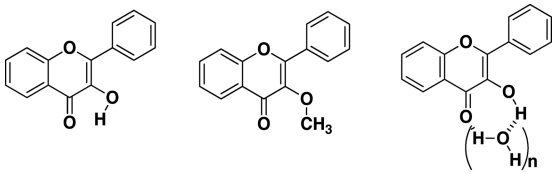

Fluorescence anisotropy (FA) is a fluorescence intensity-based ratiometric technique and therefore, to a good extent, is independent of experimental artifacts like fluctuations of light intensity and so on.[14] It is a measure of the depolarization of emitted light from a fluorophore when excited with polarized light and depends on the mutual orientations of the excitation and emission dipoles of a fluorophore.[14] FA principally deals with the rotational intricacies of a fluorophore in free as well as in any type of bound or aggregated state.[14] In most of the solvents of low viscosity, a fluorophore in its photoexcited state rotates freely within its fluorescence lifetime, resulting in a very low FA. However, enhancement in the viscosity of the medium or some specific interaction of the fluorophore with the environment or any type of aggregation interaction often leads to an increased FA value.[14−19] Thus, FA is sensitive toward the effective volume and the structural aspect of the emitting

Received: August 8, 2019
Revised: October 17, 2019
Published: October 17, 2019

DOI: 10.1021/acs.jpcb.9b07526
J. Phys. Chem. B 2020, 124, 173−180

species. Apart from providing fundamental information about the fluorophores, now, the technique is also being exploited in contemporary therapeutic research for imaging purposes.[20,21]

To contribute to the yet unexplored field of FA of 3HF, we recently demonstrated, for the first time, that 3HF reveals unprecedented high FA in protic solvents, especially in water, contrary to the very low FA of 3-methoxyflavone (3MF) (Scheme 1), the methoxy counterpart of 3HF lacking the hydroxyl proton, in the same experimental conditions.[22] To rationalize the observation, we proposed formation of an intermolecularly hydrogen-bonded cage-like probe−solvent cluster (Scheme 1) to be responsible for the unusual behavior of 3HF.[22] This has been, later on, supported by several groups.[23−26] In apolar aprotic solvents, however, FA of 3HF is reported to be very low, as expected.[22]

Considering the importance of the atypical solvation of 3HF in water, in the present work, endeavors have been made to substantiate our proposition from the theoretical point of view as well as to find the number of water molecules involved in the probe−solvent cluster formation at equilibrium. It is observed that the stabilization energy of different 3HF−water clusters passes through a minimum with four to five water molecules, which thereby provides a strong foundation for the formation of a solvated cluster of 3HF in water. Molecular dynamics simulations also demonstrate that the rotational dynamics of 3HF is slowed down appreciably in water relative to that in hexane medium, which also corroborates the unusual interaction of the probe with the surrounding water molecules. In addition to the theoretical studies, an indirect experimental approach of introducing anionic micelles of varying surfactant chain lengths incorporating the probe is adopted to substantiate our original proposition of formation of a 3HF−water cage-like cluster in aqueous medium.

2. MATERIALS AND METHODS

2.1. Experimental Section. 3-Hydroxyflavone (Fluka, USA) and 3-methoxyflavone (TCI, Japan) were used as received after confirming their purity from their absorption, fluorescence, and fluorescence excitation spectra in the reported solvents. Sodium octyl sulfate (S_8S), sodium decyl sulfate ($S_{10}S$), sodium dodecyl sulfate ($S_{12}S$), and sodium tetradecyl sulfate ($S_{14}S$) were procured from Sigma-Aldrich (USA) and used without further purification. Spectroscopic-grade methanol (Sigma-Aldrich, USA) was used for the preparation of stock solutions of the probes. The volume of methanol in the final experimental solutions was <1%. Deionized water from a Milli-Q water purification system (Millipore) was used throughout the experiment. Fresh solutions of probe and surfactants were used for the experiments. All the experiments were performed in 20 mM phosphate−citrate buffer at pH 3.5.

A Horiba Jobin Yvon Fluoromax-4 spectrofluorometer was employed for the steady-state fluorescence and fluorescence anisotropy measurements. Fluorescence anisotropy (r) is defined as[14]

$$r = \frac{I_{VV} - G \times I_{VH}}{I_{VV} + 2G \times I_{VH}} \quad (1)$$

where I_{VV} and I_{VH} are the emission intensities obtained with the excitation and emission polarizers set at (0°, 0°) and (0°, 90°), respectively. The instrumental factor, G, is defined as[14]

$$G = \frac{I_{HV}}{I_{HH}} \quad (2)$$

where I_{HV} and I_{HH} refer to the emission signals for excitation and emission polarizers set at (90°, 0°) and (90°, 90°), respectively.

Time-resolved FA decay measurements were performed in a Horiba Jobin Yvon DeltaFlex TCSPC fluorescence lifetime system equipped with polarizers. DeltaDiodes at 330 and 370 nm were used as excitation sources, and a PPD-900 photon detection module served as the detector. The anisotropy decay functions were constructed following the standard procedure[14,15] and analyzed with the EZ-time software provided with the instrument.

Dynamic light scattering (DLS) measurements were performed on a Nano-ZS90 Malvern instrument (Model DLS-nano ZS, Zetasizer, Nano series) equipped with a 4 mW He−Ne laser (λ = 632.8 nm) and a thermostatically controlled sample chamber. Samples were filtered with a 0.1 μm syringe filter (Merck Millipore Ltd.) prior to the measurements. For each measurement, the mean was taken over 20 runs with fresh sample solutions and each run was averaged for 20 s.

For the surface tension measurements of the surfactant solutions, a tensiometer (Jencon, India, Sl. no. 259) was used.

2.2. Computational Section. Quantum chemical calculations were performed using Gaussian 09 software[27] for obtaining the energy-minimized structure of 3HF and 3HF−water cage-like structures. Energies of the organized water clusters were separately obtained from single-point calculations of the cage-like structure without 3HF. The ground-state calculations were carried out at a density functional theory (DFT) level with Becke's three-parameter hybrid functional B3 with nonlocal correlation of Lee−Yang−Parr (LYP) abbreviated as B3LYP[28,29] and 631+G** basis sets. The polarizable continuum model of the integral equation formalism variant (IEFPCM)[30−32] was employed as the solvent model to evaluate the effect of solvent on the structures.

The atomistic molecular dynamics (MD) simulations were carried out using the Gromacs software suite (version 2018.6).[33] Two separate systems were simulated: a system containing one 3HF molecule in (i) water and (ii) hexane and a system of 3MF in hexane. The 3HF molecule was solvated in a cubic box of length 4 nm with periodic boundary conditions in all directions. The GAFF force field was adopted for 3HF, 3MF, and hexane, and the TIP3P model was used for water.[34,35] The partial charges were derived using standard RESP fitting of the electrostatic potential computed at the HF/6-31G* level of theory.[36] The temperature and pressure were maintained at 300 K and 1 atm, respectively, using a velocity rescale thermostat and a Parrinello-Rahman barostat.[37,38] After an equilibration phase of 2 ns, the production trajectory was continued for 50 ns and frames were saved every 100 fs.

3. RESULTS AND DISCUSSION

3.1. Quantum Chemical Calculation. The purpose of performing DFT-based quantum chemical calculation was to find out whether or not 3HF forms energetically stable cage-like or loop-like structures as originally proposed by us to substantiate its high FA (~0.30) in aqueous medium.[22] We were also interested in finding the number of water molecules involved in the most stable structure of the 3HF−water cluster.

Since the emission from the enol form of 3HF exhibits high FA (FA of the emission from the keto form is ~0.07),[22] for the

DOI: 10.1021/acs.jpcb.9b07526
J. Phys. Chem. B 2020, 124, 173−180

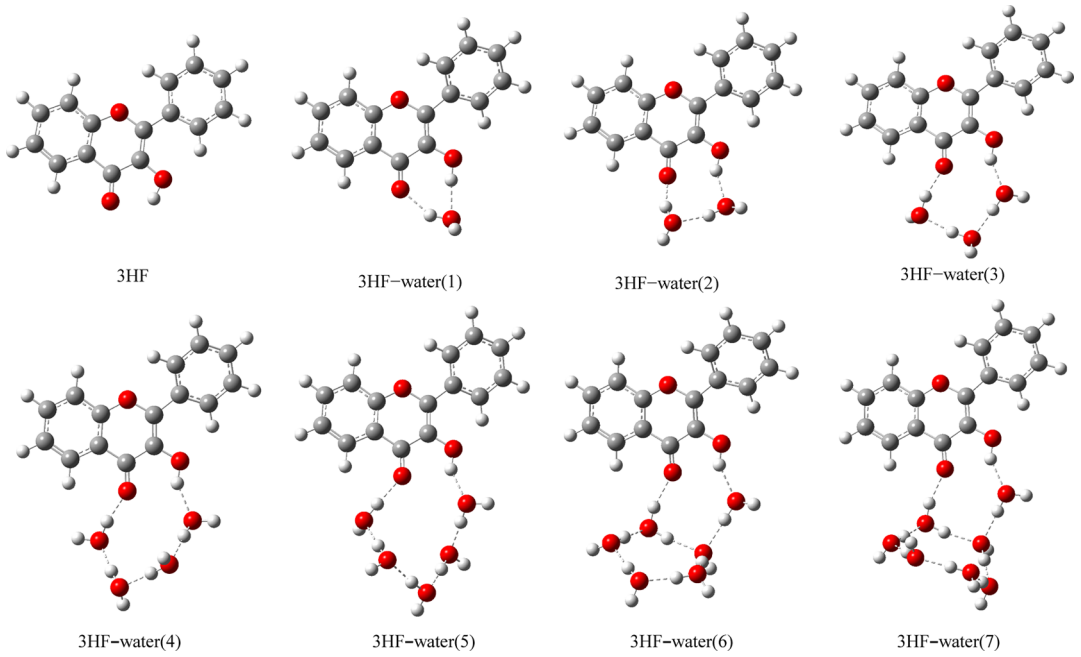

Figure 1. Energy-minimized structures of 3HF and its aquated clusters with one to seven water molecules (number of water molecules involved in the cluster formation is given in parentheses). Atomic notations: gray, carbon; off-white, hydrogen; red, oxygen.

entire study, we have focused on this form only. First, the enol form of 3HF was optimized in the ground state using water as solvent, and the corresponding optimized geometry is portrayed in Figure 1. Then, taking its output, one water molecule was put in such a fashion that the hydroxyl proton and the carbonyl oxygen of 3HF remained within the hydrogen-bonding distance of the water molecule and the whole structure was optimized again following the same procedure. After this, removing the 3HF molecule from the optimized structure of 3HF−water(1) (the number within the parenthesis represents the number of water in the probe−water cluster), the water molecule was kept as it was and then its single point energy was calculated. Now, to calculate the stabilization energy of the 3HF−water(1) cluster, the respective energies of 3HF and the water molecule were subtracted from that of the 3HF−water(1) cluster. For the 3HF−water(2) cluster, an additional water molecule was placed in close proximity of the water molecule of the 3HF−water(1) cluster in such a way that both the water molecules stayed within the hydrogen bonding distance of the carbonyl oxygen and hydroxyl proton of 3HF forming a closed loop or cage. Then, the entire structure was optimized, and after optimization, the single-point energy of two water molecules was calculated removing 3HF. The stabilization energy of the 3HF−water(2) cluster was determined following the procedure as applied for the 3HF−water(1) cluster. Thus, the entire procedure was extended for more than two water molecules, and for the present case, the number of water molecules was increased up to 7, forming closed-loop or cage-like structures involving 3HF and water molecules. The corresponding stabilization energies of 3HF−water(n) clusters (n = 1, 2, 3,...7) were determined using eq 3. The energy-optimized geometries of 3HF−water clusters are depicted in Figure 1, and their stabilization energies are plotted against the number of water molecules and portrayed in Figure 2.

$$\text{stabilization energy}(\Delta E) = E_{\text{3HF−water}(n)\text{cluster}}(E_A) - E_{\text{water}(n)\text{cluster}}(E_B) - E_{\text{3HF}} \quad (3)$$

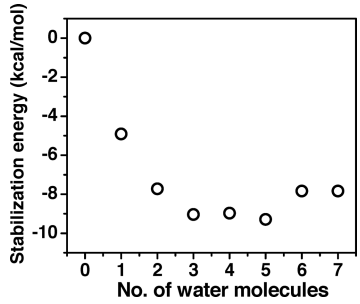

Figure 2. Stabilization energy of the 3HF−water cluster as a function of number of water molecules in the cluster.

where $E_{\text{3HF−water}(n)\text{ cluster}}$ denotes the overall optimized energy of "n" water molecules forming the cluster with 3HF, $E_{\text{water}(n)\text{ cluster}}$ is the single-point energy of "n" organized water molecules without 3HF, and E_{3HF} is the optimized energy of 3HF alone. The detailed energy calculations are provided in Table S1 in the Supporting Information. It is pertinent to mention here that, for this calculation, a continuum model of water was used as an approximation of the bulk water surrounding the 3HF−water clusters. For the justification of the loop-like positioning of the water molecules within the hydrogen-bonding distance of the carbonyl oxygen and hydroxyl proton of 3HF, the following explanation can be given. Looking at the structure of 3HF (Scheme 1), it is observed that apart from the carbonyl oxygen, 3-hydroxy group, and the ring oxygen, the rest of the molecule is hydrophobic in nature. Moreover, the ring oxygen of 3HF is unable to take part in the formation of any loop-like structure with water molecules. Therefore, the only possible way to form

DOI: 10.1021/acs.jpcb.9b07526
J. Phys. Chem. B 2020, 124, 173−180

a closed-loop-like structure with water molecules and 3HF is to involve the abovementioned hydrogen-bonding centers of the probe, the carbonyl oxygen and 3-hydroxyl proton. The importance of the 3-hydroxyl proton in high FA of 3HF has already been established while comparing with the very low FA of 3MF lacking the 3-hydroxyl proton.[22]

Figure 2 reveals that the stabilization energy of 3HF−water clusters as a function of increasing number of associated water molecules passes through a minimum. This trend can be rationalized by the following explanation. The carbonyl and hydroxyl groups of 3HF provide an optimal geometry for participation in intermolecular hydrogen bonding with water molecules so that a loop-like arrangement of water molecules is stabilized. With the increase in the number of water molecules in the 3HF−water cluster, the overall stabilization continues to increase up to four to five water molecules (Figure 2). Addition of water molecules beyond five leads to enhanced bulkiness of the entire 3HF−water cluster, and the single loop-like structure is not sustained (3HF−water(6) in Figure 1). It is observed that, instead of forming one loop-like structure comprising 3HF and water molecules, two interconnected loops are formed to maximize the number of hydrogen bonds between the water molecules themselves,[39,40] leading to a decrease in the overall stability of the cluster. Thus, the trend of stabilization energies of 3HF−water clusters suggests that 3HF indeed forms intermolecular hydrogen-bonded probe−water clusters containing four to five water molecules and therefore provides a strong foundation in favor of our proposition of formation of the 3HF−water cluster.[22] This 3HF−water cluster is attributed to be responsible for the unusually high FA of 3HF in water since it results in a remarkable increase in the effective size of the solvated probe compared to bare 3HF.[22] As expected, for 3MF, the stabilization energies with varying numbers of water molecules were very small compared to the situations of 3HF, principally because of the methyl substitution of the hydroxyl proton that limits the formation of additional H bonding with the solvent.

It is pertinent to mention here that in our first attempt of this sort, we have only considered the immediate organized layer of water around the probes (3HF and 3MF). Assuming that the higher-order solvation shells would grow around the first shell, we were mainly interested in monitoring the first solvation shell. Our calculation reveals an appreciable enhancement in the effective size of the solvated 3HF (taking the first shell only). We also expect a similar effect to propagate with higher solvation shells. In this first endeavor, we have tried to explore the differential modification of the first solvation shell of the two probes 3HF and 3MF. The only difference between 3HF and 3MF molecules is in the replacement of the hydroxyl (−OH) group by a methoxy ($-OCH_3$) group. Thus, it is likely that the observed difference in FA originates from the local structuring of water around the carbonyl and hydroxyl groups of 3HF. Our objective was to investigate the presence of any special water structuring around this specific region of 3HF, and indeed we find the presence of a chain/loop-like structure of hydrogen-bonded water molecules that connects the carbonyl and hydroxyl groups. Such structuring involving the hydroxyl group would not be possible in the case of 3MF.

3.2. Molecular Dynamics Simulation. It is known that the FA of a fluorophore effectively depends on its excited state.[14] Therefore, to properly deal with the FA of a probe from theoretical point of view, ideally, one should perform the entire calculation using the excited-state geometry and consider the ensemble average of the second Legendre polynomial involving the absorption and emission dipoles.[14,41] However, due to the demanding computational cost of rigorous time-dependent excited-state calculations, we have performed the atomistic classical MD simulations using the ground-state dipole of 3HF to support our proposition of formation of the cage-like 3HF−water clusters through a comparison of dynamics of the probe in water and hexane media (Figure 3). Since in 3MF the hydroxyl proton is

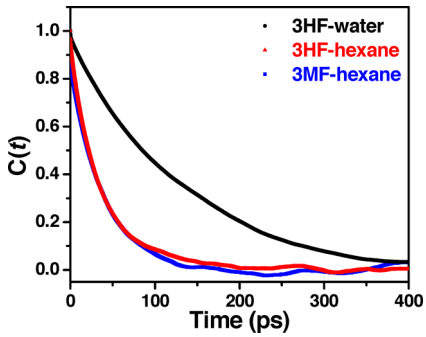

Figure 3. Dipole orientational correlation function ($C(t)$) for 3HF in water and 3HF and 3MF in hexane.

replaced by a methyl group, there is no scope of formation of the probe−water loop-like structure like the one feasible for 3HF in water. However, to justify the similar (low) FA values of 3HF and 3MF in alkane medium, the MD simulation of 3MF in hexane is presented (Figure 3). The rotational dynamics of the probes are measured in terms of the orientational correlation function as defined below

$$C(t) = \langle \mu(0) \cdot \mu(t) \rangle \tag{4}$$

where $\mu(t)$ is the unit vector along the ground-state dipoles of the probes at time t. The $\langle\rangle$ symbol indicates the ensemble average over the MD trajectory. The comparison between the correlation function in water and hexane is shown in Figure 3. The calculated $C(t)$ data are fitted to a bi-exponential function ($C(t) = a_1 \exp(-t/t_1) + a_2 \exp(-t/t_2)$), and the fitting parameters are reported in Table 1. The number of exponential

Table 1. Dipole Orientational Time Correlation Function Fitting Parameters of 3HF in Water and 3HF and 3MF in Hexane

system	a_1	t_1 (ps)	a_2	t_2 (ps)	t_{avg} (ps)
3HF/water	0.02	0.1	0.98	125.8	123.3
3HF/hexane	0.39	16.0	0.61	49.7	36.6
3MF/hexane	0.15	0.4	0.85	38.5	32.8

terms was determined by the minimum number of exponential terms required to capture all distinct time-scales as well as the quality of the fitting (measured by correlation coefficient and χ^2 values). The average rotational time (t_{avg}) was calculated as[14]

$$t_{avg} = a_1 t_1 + a_2 t_2 \tag{5}$$

From Table 1, we observe that, in water, the average time for orientational motion of 3HF is 123.3 ps, which is ∼3.4 times slower than the corresponding time in hexane (36.6 ps). While the ground-state rotational dynamics is not quantitatively equivalent to the anisotropy decay process, it is still quite

DOI: 10.1021/acs.jpcb.9b07526
J. Phys. Chem. B 2020, 124, 173−180

evident that the hydrogen bonding network present in a protic solvent like water dramatically slows down the rotational motion of 3HF as compared to a non-polar solvent like hexane. As expected, in alkane solvent, the average rotational time of 3HF agrees with that of 3MF. The MD simulations, thus, justify and strengthen our proposition of formation of a hydrogen-bonded solvated cluster of 3HF in water.

3.3. Steady-State Fluorescence Anisotropy Study. After acquiring encouraging support from theoretical studies, our intention was to provide further experimental evidence in favor of our original proposition.[22] To materialize this, we have purposefully disrupted the 3HF−water cage-like structure by introducing surfactants of varying surfactant chain length and eventually entrapped the fluorophore in the respective anionic micelles. We have studied the modulation of the FA of 3HF in these experimental environments using steady-state and time-resolved spectroscopic techniques, being aware of the fact that the aspect of excited-state intramolecular proton transfer (ESIPT) of 3HF has already been carried out by other groups in such media.[6,10] To avoid any perturbation from the emission of the photoproduced anion of the probe in the anionic micellar media,[10] we have performed the entire study in phosphate−citrate buffer medium at pH 3.5. The emission profile of 3HF and the FA values in the buffer medium are, however, found to remain similar to those observed in pure aqueous medium.

Figure 4 depicts the variation patterns of FA of 3HF as a function of concentration of various sodium *n*-alkyl sulfate

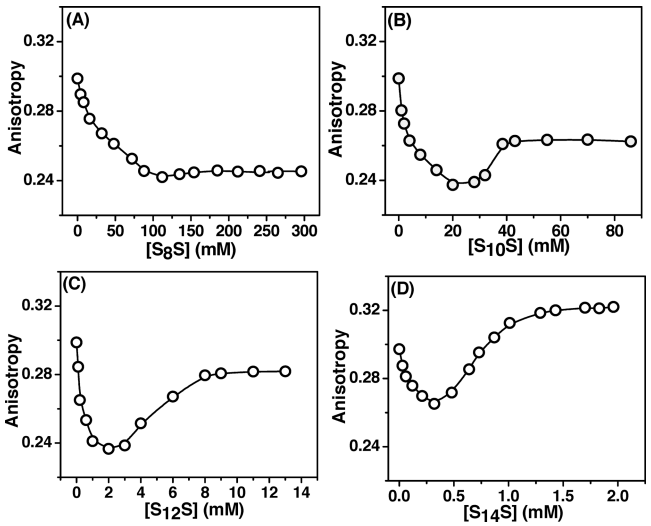

Figure 4. FA of 3HF as a function of concentration of (A) S_8S, (B) $S_{10}S$, (C) $S_{12}S$, and (D) $S_{14}S$. λ_{ex} = 345 nm and $\lambda_{monitored}$ = 405 nm. [3HF] ≈ 4 μM. Average of 20 consistent anisotropy values is presented for every concentration of S_nSs.

(S_nS) (n = 8, 10, 12, and 14) surfactants. As a sharp contrast to the normally observed increasing trend of the FA values of most of the fluorophores with the gradual addition of surfactants, the FA of 3HF shows an initial decrease followed by an increase, passing through the respective minima. The pattern of variation is found to be similar in all the S_nS micellar systems, which reflects the consistency and hence reliability of our work.

Variation of the FA values of 3HF with the addition of different surfactants is rationalized by the combined effect of two opposing factors: one decreasing and the other increasing. The interaction of the initially solvated probe with the surfactant monomers in the pre-micellar region[42,43] leads to disruption of the probe−water cluster, resulting in a lowering of the FA. This indirectly corroborates the existence of the 3HF−water cluster. The increasing factor comes from the micelle-bound probe where, due to the enhanced effective size and motional restriction in the micellar environments, the FA value increases. Hence, the plot of FA against concentration of the surfactant passes through a minimum for each of the S_nS systems. It is obvious that in the pre-micellar region, the disruption of the solvated probe dominates. However, on exceeding the respective critical micellar concentrations (CMCs), the increasing population of the organized micellar assemblies helps to surpass the lowering of FA of the fluorophore and augments the FA afterward. The FA of the probe in different micellar media attains respective saturation values when a sufficient amount of micelles is formed. As the micelles become bigger in size with increasing chain length of the surfactants,[44,45] the effective dimensions of the micelle-bound probe increase, justifying the increasing trend of FA values of 3HF in the studied micellar systems at the respective saturations. The relative FA values at the plateaus of the respective plots compared to the value in buffer medium give a relative measure of the dimension of the micelle-bound probe to the aquated probe. Experimental results reveal that 3HF bound to the $S_{14}S$ micelle has a larger dimension than the solvated probe in water, whereas in other studied S_nS micelles, the sizes are smaller (see later). A clear increasing trend of the saturation values of the anisotropy is observed with increasing chain length of the surfactants, indicating the increasing size of the micelles from S_8S to $S_{14}S$ (Table 2 and Figure 5A, see later). It is interesting to note that the saturation anisotropy values of 3HF in the micellar environments fail to surpass that in the buffer medium with $S_{14}S$ being the only exception. It is

Table 2. Hydrodynamic Diameters and the Steady-State FA Values of 3HF in Different Media

medium	hydrodynamic diameter of 3HF (± 0.4 nm)	steady-state FA (± 0.005)
buffer	5.4	0.299
S_8S (296 mM)	3.6	0.245
$S_{10}S$ (75 mM)	4.1	0.263
$S_{12}S$ (12 mM)	4.8	0.282
$S_{14}S$ (1.5 mM)	5.5	0.321

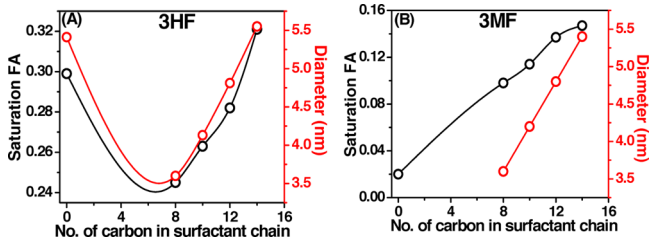

Figure 5. Variation of saturation FA values (black, left axis) and hydrodynamic diameters (red, right axis) of (A) 3HF and (B) 3MF in buffer and different S_nS micellar media. In panel (B), the diameter of 3MF is not obtained in the buffer medium as it falls below the instrumental resolution limit (1.0 nm) (see later). The solid line is only to guide the eyes.

DOI: 10.1021/acs.jpcb.9b07526
J. Phys. Chem. B 2020, 124, 173−180

noteworthy that the FA values of 3HF at the respective minima in the S_nS micelles are quite similar except for $S_{14}S$ (Figure 4) where FA is appreciably higher. Since among the studied micellar systems in aqueous buffer, $S_{14}S$ has the lowest CMC value (~0.3 mM) and the highest aggregation number (75),[16] a smaller number of micelles in the $S_{14}S$ system appears to be insufficient to accommodate all the 3HF molecules present in the solution. This leads to the fact that some of the unbound probe molecules still remain aquated in the form of the aforesaid cluster. Since these clusters exhibit higher anisotropy, we see a higher value of FA at the CMC in the case of $S_{14}S$ micelle. The enhanced viscosity of the medium due to the presence of $S_{14}S$ might also be attributed to the increased FA of 3HF at the minimum.

The surfactant concentrations at which the FA value of 3HF reaches the minimum in the surfactant solutions correspond to the CMCs of the respective micelles in the experimental buffer solutions. The CMC values agree well with the values determined from the surface tension measurements (Figure S1 and Table S2 in the Supporting Information). Thus, the work provides a simple way of determination of the CMCs of micelles through FA measurements.

To establish the impact of disruption of the probe−water network of 3HF in the presence of micelles, we have extended our study to 3MF, the methoxy counterpart of 3HF, in the same S_nS micellar environments (Figure S2 in the Supporting Information). For 3MF, the very low FA in buffer medium rules out formation of any type of probe−solvent cluster, as already reported.[22] A glance of Figure 4 and Figure S2 categorically reveals the difference between the variation patterns of FA of 3HF and 3MF in aqueous medium with the gradual addition of different surfactants. The saturation FA values of 3MF in all the studied micelles are higher than the anisotropy value of the probe in aqueous medium, as normally expected. Due to the increased micellar size, the saturation FA value of micelle-entrapped 3MF increases with an increase in the surfactant chain length (Figure 5B). Interestingly, the trends of variation of saturation FA against the surfactant chain length of the S_nS micelles for 3HF (Figure 5A) and 3MF (Figure 5B and Table S3) are very different when considered in reference to the respective FA values of the probes in aqueous buffer medium. It is noteworthy that the dimensions (obtained from DLS measurements) of 3HF and its methoxy derivative in these studied S_nS media including those in buffer medium follow a similar trend to that observed for their saturation FA (Figure 5). The lower saturation values of FA of 3HF in S_8S, $S_{10}S$, and $S_{12}S$ media with respect to that in aqueous buffer, in fact, highlight disruption of the solvated cluster of the probe in the presence of the micellar media, leading to a reduction in the effective size of the probe. Except for $S_{14}S$, the lower saturation values of FA of 3HF in other studied S_nS media relative to the FA of the probe in water medium corroborate our earlier observations in the presence of other supramolecular assemblies.[46,47] Lowering of the FA values in these media is rationalized from the smaller dimensions of the supramolecule-bound probe compared to the dimension of the probe−water cluster. Breaking of the probe−water cluster is also supported from our observation of the reduced FA of 3HF in water upon addition of water structure breakers (chaotropes) like urea or guanidine hydrochloride.[46]

3.4. Time-Resolved Fluorescence Anisotropy Study. To decipher the rotational intricacies of 3HF and 3MF in aqueous buffer medium and in the studied anionic micellar environments, time-resolved FA has been employed. Figure 6

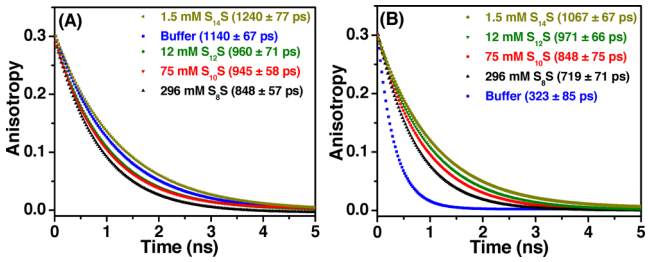

Figure 6. Fitted FA decays of (A) 3HF and (B) 3MF in different environments. λ_{ex} = 330 nm and λ_{em} = 405 nm for 3HF and λ_{ex} = 370 nm and λ_{em} = 430 nm for 3MF. Both [3HF] and [3MF] ≈ 4 μM. The legends contain the respective concentrations of S_nS and the corresponding rotational correlation times of 3HF and 3MF in different media.

depicts the anisotropy decay profiles. For the sake of clarity, only the fitted data are presented in the figure and the experimental raw data are presented in Figures S5 and S6 for 3HF and 3MF, respectively. Figure 6 portrays the fitted FA decays of 3HF and 3MF in the presence of sufficient concentrations of S_nS where the steady-state FA values of the probe have already achieved the respective saturations. Comparing the FA decays of 3HF and 3MF in buffer medium (blue decays in Figure 6A,B), it is observed that the decay of 3HF is visibly much slower than that of 3MF. This result parallels to the observation as obtained from the steady-state FA studies, justifying the retarded motion of the solvated 3HF in buffer medium relative to its counterpart, 3MF. Moreover, the anisotropy decays of 3HF in S_8S, $S_{10}S$, and $S_{12}S$ micelles are relatively faster than that in pure buffer medium, which is opposite to the generally observed increasing rotational correlation times for other fluorophores in general, similar to the case of the methoxy analogue of 3HF here (Figure 6B).

Breakdown of the solvated structure of 3HF is attributed accountable for this unorthodox observation of the FA decays of the same in the studied S_nS micellar media relative to that of the probe in buffer medium. The order of the rotational correlation times of 3HF in the studied media follows S_8S < $S_{10}S$ < $S_{12}S$ < buffer < $S_{14}S$ corresponds to the findings from the steady state measurements putting our explanations on a firm base.

3.5. Dynamic Light Scattering Study. Since FA of a probe is very much dependent on its effective size in a fluid medium,[14] we have determined dimensions of the solvated 3HF in the studied media exploiting the technique of dynamic light scattering (DLS). The hydrodynamic diameter of 3HF in buffer medium is found to be 5.4 nm that agrees well with our earlier reports.[22,46,47] The diameters of micellized 3HF in the studied S_nS systems are measured at surfactant concentrations where the steady state FA reaches the individual saturations. In a comparative approach, the distributions of diameter of 3HF in the S_nS micellar media along with that in aqueous buffer are depicted in Figure S3(A) in the Supporting Information and the hydrodynamic diameters of 3HF in these environments are recorded in Table 2. From Table 2, it is evident that with the increase in the hydrocarbon chain of the surfactants, overall size of the micellized 3HF increases in the investigated S_nS environments corroborating our steady state and time resolved FA data. This is rationalized taking into account the increasing

DOI: 10.1021/acs.jpcb.9b07526
J. Phys. Chem. B 2020, 124, 173−180

surfactant chain lengths as well as the aggregation numbers of the surfactants ranging from S_8S to $S_{14}S$.[42] A correspondence between the FA values of 3HF in the S_nS media and the respective dimensions of 3HF in these micellar environments has also been observed (Figure S3(B) in the Supporting Information) which might serve the good purpose of size-anisotropy relationship for the probe in the S_nS micellar environments. Upon applying the DLS technique to 3MF in aqueous buffer, it fails to provide any characteristic peak since its dimension remains below the resolution limit (1.0 nm) of our instrument. The low FA value of 3MF and its smaller dimension corroborate each other. However, when the study with 3MF is extended in different S_nS media, the dimensions of micelle-bound 3MF are found to be comparable to the dimensions of the probe-free micelles, following the order $S_8S < S_{10}S < S_{12}S < S_{14}S$ (Figure S4 and Table S3 in the Supporting information) corroborating the steady state FA data for the said probe in the studied micelles. Analogous trends of variation of dimensions of the probes and their FA values in different media, varying from buffer to $S_{14}S$ through S_8S, $S_{10}S$ and $S_{12}S$ (Figure 5) also reveal the reliability of our experiments.

4. CONCLUSIONS

The present work, consisting of both theory and experiments, provides a strong foundation to our original proposition of formation of a 3HF−water cage-like cluster in rationalizing the unusually high fluorescence anisotropy of the probe. Exploiting ab initio quantum chemical calculations, it has been made clear that 3HF indeed forms a solvated cluster in aqueous medium and four to five water molecules are intermolecularly hydrogen-bonded with 3HF in a cooperative way. Formation of such clusters is assigned to be responsible for its larger effective dimension and consequently its atypical high-fluorescence anisotropy in aqueous medium. Molecular dynamics simulation also reveals that the rotational dynamics of 3HF in aqueous medium is remarkably slower compared to that in nonpolar alkane medium, supporting formation of the probe−water cage-like structure. Further, the unusual decrease of FA of 3HF has been demonstrated in the presence of anionic S_nS surfactants relative to that in the buffer medium, which is in sharp contrast to the increasing trend of the same for other probes like the methoxy analogue of 3HF in similar situations. Due to the specific interaction of the aquated cluster of 3HF with the surfactants in the pre-micellar region, disruption of the solvated network of the probe takes place resulting in a decrease in the FA value, thereby indirectly validating our proposition of formation of an intermolecularly hydrogen-bonded probe−water cluster. These unique and unusual observations obtained through a combined venture of theoretical and experimental studies undoubtedly reveal that there is much more to explore in the field of solvation and it has the potential to unravel a new dimension in the said arena.

■ ASSOCIATED CONTENT

Supporting Information

The Supporting Information is available free of charge at https://pubs.acs.org/doi/10.1021/acs.jpcb.9b07526.

Calculation of stabilization energies of 3HF−water clusters, tensiometric determination of CMCs of S_nS micelles and their comparison with experimentally obtained CMCs from fluorescence anisotropy measurement, variation of fluorescence anisotropy of 3MF as a function of concentration of S_nS micelles, size distribution of 3HF and 3MF in different environments, and raw data of time-resolved FA decay of both 3HF and 3MF in different environments (PDF)

■ AUTHOR INFORMATION

Corresponding Author

*E-mail: nitin.chattopadhyay@yahoo.com. Fax: 91-33-2414-6584.

ORCID

Sinjan Das: 0000-0001-6269-128X

Suman Chakrabarty: 0000-0002-9461-0015

Nitin Chattopadhyay: 0000-0002-4103-0199

Notes

The authors declare no competing financial interest.

■ ACKNOWLEDGMENTS

The authors gratefully acknowledge the financial support from the Department of Science and Technology, India (project no. EMR/2016/001087). S.D. thanks the University Grants Commission, New Delhi for his Senior Research Fellowship. S.C. thanks S. N. Bose National Centre for Basic Sciences, Kolkata for the computational facility and the Department of Science and Technology, India for funding (project no. ECR/2018/002903). The authors are thankful to Prof. Subhash Chandra Bhattacharya and Prof. Ambikesh Mahapatra of the same department of J.U. for extending the DLS and the tensiometer facilities, respectively.

■ REFERENCES

(1) Sengupta, P. K.; Kasha, M. Excited State Proton-Transfer Spectroscopy of 3-Hydroxyflavone and Quercetin. *Chem. Phys. Lett.* **1979**, *68*, 382−385.

(2) Woolfe, G. J.; Thistlethwaite, P. J. Direct Observation of Excited State Intramolecular Proton Transfer Kinetics in 3-Hydroxyflavone. *J. Am. Chem. Soc.* **1981**, *103*, 6916−6923.

(3) McMorrow, D.; Kasha, M. Proton-Transfer Spectroscopy of 3-Hydroxyflavone in an Isolated-Site Crystal Matrix. *Proc. Natl. Acad. Sci. U. S. A.* **1984**, *81*, 3375−3378.

(4) McMorrow, D.; Kasha, M. Intramolecular Excited-state Proton Transfer in 3-Hydroxyflavone. Hydrogen-Bonding Perturbations. *J. Phys. Chem. B* **1984**, *88*, 2235−2243.

(5) Dick, B. AM1 and INDO/S Calculations on Electronic Singlet and Triplet States Involved in Excited-State Intramolecular Proton Transfer of 3-Hydroxyflavone. *J. Phys. Chem.* **1990**, *94*, 5752−5756.

(6) Sarkar, M.; Sengupta, P. K. Influence of Different Micellar Environments on the Excited-State Proton-Transfer Luminescence of 3-Hydroxyflavone. *Chem. Phys. Lett.* **1991**, *179*, 68−72.

(7) Guharay, J.; Chaudhuri, R.; Chakrabarti, A.; Sengupta, P. K. Excited State Proton Transfer Fluorescence of 3-Hydroxyflavone in Model Membranes. *Spectrochim. Acta A* **1997**, *53*, 457−462.

(8) Klymchenko, A. S.; Demchenko, A. P. Probing AOT Reverse Micelles with Two-Color Fluorescence Dyes Based on 3-Hydroxychromone. *Langmuir* **2002**, *18*, 5637−5639.

(9) Banerjee, A.; Sengupta, P. K. Encapsulation of 3-Hydroxyflavone and Fisetin in β-Cyclodextrins: Excited State Proton Transfer Fluorescence and Molecular Mechanics Studies. *Chem. Phys. Lett.* **2006**, *424*, 379−386.

(10) Mondal, S.; Basu, S.; Mandal, D. Ground- and Excited-State Proton-Transfer Reaction of 3-Hydroxyflavone in Aqueous Micelles. *Chem. Phys. Lett.* **2009**, *479*, 218−223.

(11) Jana, B.; Senapati, S.; Ghosh, D.; Bose, D.; Chattopadhyay, N. Spectroscopic Exploration of Mode of Binding of ctDNA with 3-Hydroxyflavone: A Contrast to the Mode of Binding with Flavonoids

DOI: 10.1021/acs.jpcb.9b07526
J. Phys. Chem. B 2020, 124, 173−180

Having Additional Hydroxyl Groups. *J. Phys. Chem. B* **2011**, *116*, 639−645.
(12) Ghosh, S.; Chattopadhyay, N. Modification of the Photophysics of 3-Hydroxyflavone in Aqueous Solutions of Imidazolium-Based Room Temperature Ionic Liquids: A Comparison between Micelle-Forming and Non Micelle-Forming Ionic Liquids. *RSC Adv.* **2015**, *5*, 49054−49061.
(13) Rice-Evans, C. Flavonoid Antioxidants. *Curr. Med. Chem.* **2001**, *8*, 797−807.
(14) Lakowicz, J. R. *Principles of Fluorescence Spectroscopy*; 3rd Ed.; Springer: New York, 2006.
(15) Das, P.; Mallick, A.; Sarkar, D.; Chattopadhyay, N. Probe-Induced Self-Aggregation of γ-Cyclodextrin: Formation of Extended Nanotubular Suprastructure. *J. Phys. Chem. C* **2008**, *112*, 9600−9603.
(16) Kundu, P.; Ghosh, S.; Das, S.; Chattopadhyay, N. Cyclodextrin Induced Controlled Delivery of a Biological Photosensitizer from a Nanocarrier to DNA. *Phys. Chem. Chem. Phys.* **2016**, *18*, 3685−3693.
(17) Afzal, M.; Ghosh, S.; Das, S.; Chattopadhyay, N. Endogenous Activation-Induced Delivery of a Bioactive Photosensitizer from a Micellar Carrier to Natural DNA. *J. Phys. Chem. B* **2016**, *120*, 11492−11501.
(18) Kaiser, T. E.; Wang, H.; Stepanenko, V.; Würthner, F. Supramolecular Construction of Fluorescent J-Aggregates Based on Hydrogen-Bonded Perylene Dyes. *Angew. Chem., Int. Ed.* **2007**, *46*, 5541−5544.
(19) Ray, A.; Das, S.; Chattopadhyay, N. Aggregation of Nile Red in Water: Prevention through Encapsulation in β-Cyclodextrin. *ACS Omega* **2019**, *4*, 15−24.
(20) Jameson, D. M.; Ross, J. A. Fluorescence Polarization/Anisotropy in Diagnostics and Imaging. *Chem. Rev.* **2010**, *110*, 2685−2708.
(21) Vinegoni, C.; Feruglio, P. F.; Gryczynski, I.; Mazitscheck, R.; Weissleder, R. Fluorescence Anisotropy Imaging in Drug Discovery. *Adv. Drug Delivery Rev.* (in press).
(22) Das, S.; Ghosh, S.; Chattopadhyay, N. Unprecedented High Fluorescence Anisotropy in Protic Solvents: Hydrogen Bond Induced Solvent Caging? *Chem. Phys. Lett.* **2016**, *644*, 284−287.
(23) Dey, N.; Bhattacharya, S. Mimicking Multivalent Protein−Carbohydrate Interactions for Monitoring the Glucosamine Level In Biological Fluids and Pharmaceutical Tablets. *Chem. Commun.* **2017**, *53*, 5392−5395.
(24) Li, D.; Xing, Y.; Ding, L.; Wu, C.; Hou, G.; Song, B. Tuning the Emission of a Water-Soluble 3-Hydroxyflavone Derivative by Host−Guest Complexation. *Soft Matter* **2018**, *14*, 4231−4237.
(25) Lazzaroni, S.; Dondi, D.; Mezzetti, A.; Protti, S. Role of Solute-Solvent Hydrogen Bonds on the Ground State and the Excited State Proton Transfer in 3-Hydroxyflavone. A Systematic Spectrophotometric Study. *Photochem. Photobiol. Sci.* **2018**, *17*, 923−933.
(26) Kundu, K.; Singh, A. P.; Panda, S.; Singh, V.; Gardas, R. L.; Senapati, S. Study on the Conformation of Entrapped Protein inside the Reverse Micellar Confinement Based on the Amino Acid Derived Ionic Liquid. *ChemistrySelect* **2018**, *3*, 4768−4776.
(27) Frisch, M. J.; Trucks, G. W.; Schlegel, H. B.; Scuseria, G. E.; Robb, M. A.; Cheeseman, J. R.; Scalmani, G.; Barone, V.; Mennucci, B.; Petersson, G. A., et al. *Gaussian 09*, Revision A.02; Gaussian, Inc.: Wallingford, CT, 2009.
(28) Becke, A. D. Density-Functional Thermochemistry. III. The Role of Exact Exchange. *J. Chem. Phys.* **1993**, *98*, 5648−5652.
(29) Lee, C.; Yang, W.; Parr, R. G. Development of the Colic-Salvetti Correlation-Energy Formula into a Functional of the Electron Density. *Phys. Rev. B* **1988**, *37*, 785−789.
(30) Miertuš, S.; Scrocco, E.; Tomasi, J. Electrostatic Interaction of a Solute with a Continuum. A Direct Utilization of ab initio Molecular Potentials for the Prevision of Solvent Effects. *Chem. Phys.* **1981**, *55*, 117−129.
(31) Miertuš, S.; Tomasi, J. Approximate Evaluations of the Electrostatic Free Energy and Internal Energy Changes in Solution Processes. *Chem. Phys.* **1982**, *65*, 239−245.
(32) Pascual-Ahuir, J. L.; Silla, E.; Tuñon, I. GEPOL: An Improved Description of Molecular-Surfaces. 3. A New Algorithm for the Computation of a Solvent-Excluding Surface. *J. Comput. Chem.* **1994**, *15*, 1127−1138.
(33) Abraham, M. J.; Murtola, T.; Schulz, R.; Páll, S.; Smith, J. C.; Hess, B.; Lindahl, E. GROMACS: High Performance Molecular Simulations through Multi-Level Parallelism from Laptops to Supercomputers. *SoftwareX* **2015**, *1-2*, 19−25.
(34) Wang, J.; Wolf, R. M.; Caldwell, J. W.; Kollman, P. A.; Case, D. A. Development and Testing of a General Amber Force Field. *J. Comput. Chem.* **2004**, *25*, 1157−1174.
(35) Berendsen, H. J. C.; Grigera, J. R.; Straatsma, T. P. The Missing Term in Effective Pair Potentials. *J. Phys. Chem.* **1987**, *91*, 6269−6271.
(36) Bayly, C. I.; Cieplak, P.; Cornell, W.; Kollman, P. A. A Well-Behaved Electrostatic Potential Based Method Using Charge Restraints for Deriving Atomic Charges: The RESP Model. *J. Phys. Chem.* **1993**, *97*, 10269−10280.
(37) Bussi, G.; Donadio, D.; Parrinello, M. Canonical Sampling through Velocity Rescaling. *J. Chem. Phys.* **2007**, *126*, No. 014101.
(38) Parrinello, M.; Rahman, A. Polymorphic Transitions in Single Crystals: A New Molecular Dynamics Method. *J. Appl. Phys.* **1981**, *52*, 7182−7190.
(39) Maheshwary, S.; Patel, N.; Sathyamurthy, N.; Kulkarni, A. D.; Gadre, S. R. Structure and Stability of Water Clusters $(H_2O)_n$, n = 8-20: An Ab Initio Investigation. *J. Phys. Chem. A* **2001**, *105*, 10525−10537.
(40) Karthikeyan, S.; Singh, N. J.; Kim, K. S. Undissociated versus Dissociated Structures for Water Clusters and Ammonia-Water Clusters: $(H_2O)_n$ and $NH_3(H_2O)_{n-1}$ (n = 5, 8, 9, 21). Theoretical Study. *J. Phys. Chem. A* **2008**, *112*, 6527−6532.
(41) Paloncýová, M.; Ameloot, M.; Knippenberg, S. Orientational Distribution of DPH in Lipid Membranes: A Comparison of Molecular Dynamics Calculations and Experimental Time-Resolved Anisotropy Experiments. *Phys. Chem. Chem. Phys.* **2019**, *21*, 7594−7604.
(42) Garcia, M. E. D.; Sanz-Medel, A. Dye-Surfactant Interactions: A Review. *Talanta* **1986**, *33*, 255−264.
(43) Neumann, M. G.; Gehlen, M. H. The Interaction of Cationic Dyes with Anionic Surfactants in the Premicellar Region. *J. Colloid Interface Sci.* **1990**, *135*, 209−217.
(44) Weidemaier, K.; Tavernier, H. L.; Fayer, M. D. Photoinduced Electron Transfer on the Surfaces of Micelles. *J. Phys. Chem. B* **1997**, *101*, 9352−9361.
(45) Mahata, A.; Sarkar, D.; Bose, D.; Ghosh, D.; Das, P.; Chattopadhyay, N. Photophysics and Relaxation Dynamics of a β-Carboline Based Fluorophore in Cationic Alkyltrimethylammonium Bromide Micelles. *J. Colloid Interface Sci.* **2009**, *335*, 234−241.
(46) Das, S.; Chattopadhyay, N. Unconventional Modulation of Fluorescence Anisotropy of 3-Hydroxyflavone in Cationic Micelles. *Colloid Interface Sci. Commun.* **2017**, *16*, 10−13.
(47) Das, S.; Chattopadhyay, N. Supramolecular Inclusion-Assisted Disruption of Probe−Solvent Network. *ChemistrySelect* **2017**, *2*, 6078−6081.

DOI: 10.1021/acs.jpcb.9b07526
J. Phys. Chem. B 2020, 124, 173−180